Effect of proximity coupling of chains and planes on the penetration-depth anisotropy in $YBa_2Cu_3O_7$

W. A. Atkinson and J. P. Carbotte

Department of Physics and Astronomy, McMaster University, Hamilton, Ontario, Canada L8S 4M1

We calculate the penetration depth λ in the a, b, and c directions for a simple model of $YBa_2Cu_3O_7$. In this model there are two layers—representing a CuO_2 plane and a CuO chain—per unit cell. There is a BCS-like pairing (both s-wave and d-wave are considered) interaction localized in the CuO_2 planes. The CuO chains become superconducting at temperatures lower than T_c because of their proximity to the planes and there is an induced gap in the chains. Since the temperature dependence of the penetration depth in the b direction (along the chains) is sensitive to the size of the induced gap, the difference between the shapes of the penetration depth curves in the a and b directions reveals a great deal about the nature of the condensate in the chains. We find that in our proximity model there are always regions of the chain Fermi surface on which the induced gap is much smaller than T_c, so that the temperature dependence of λ_b is always different than that of λ_a. Experimental observations of the of the ab anisotropy show nearly identical temperature dependences. The main result of our paper, then, is that a simple proximity model in which the pairing interaction is localized to the planes, and the planes are coherently coupled to the chains cannot account for the superfluid on the chains.

I. INTRODUCTION

It is widely believed that the source of the pairing interaction which is responsible for the superconducting transition in the high-T_c cuprates lies in the CuO_2 planes, which are common to all of the cuprates. Many models which attempt to explain high-T_c superconductivity are two dimensional, which is a reflection of the assumption that the only active pieces of the crystal are the CuO_2 planes and that the remaining ions act as placeholders or as charge reservoirs. In some materials, however, there are additional layers whose behavior is not clear. In $Bi_2Sr_2CaCu_2O_8$, for example, it has been suggested that the BiO layer plays the role of a normal metal in close proximity to a superconducting material.[1]

The only materials in which there is clear evidence that the CuO_2 planes are not the only active portion of the unit cell are $YBa_2Cu_3O_7$ (Y-123), $YBa_2Cu_4O_8$ (Y-124) and their close relatives. In these materials there are quasi-one-dimensional CuO chain structures. Experiments measuring the dc resistivity,[2,3] the infrared and optical conductivity,[4] and the penetration depth in untwinned crystals[5] and ceramics[6] have found large anisotropies between the a direction (in-plane, perpendicular to the chains) and the b direction (in-plane, parallel to the chains) which suggest that substantial currents are carried along the chains in both the normal and superconducting state.

In the superconducting state, the source of the condensate on the chains in unclear. One possibility is that the pairing interaction is localized to the CuO_2 planes, but that the chains become superconducting by a proximity effect. In the proximity effect, an intrinsically normal metal which is in close contact with a superconductor becomes superconducting near the junction as a result of pair tunneling through the junction. The size of the induced gap in the normal metal depends on the strength of the coupling across the junction. Y-123 and Y-124 are good candidates for proximity effect models because they have the least anisotropy between the in-plane and c axis transport properties of the cuprate superconductors, and should therefore have a relatively large coupling between the chains and planes.

Proximity effect models have been studied in the context of high-T_c materials for a number of years. The most common point of view is that the unusual properties of the cuprates can be explained by an isotropic BCS pairing interaction which is contained in one of the planes.[1,7-12] The idea behind most of the work is that although the pairing interaction may be inherently isotropic, the strongly anisotropic band structure leads to a gap structure which may account for the unusual superconducting properties of the cuprates. The current authors have taken a different point of view in recent work on proximity effect models.[13-15] We have assumed that the pairing interaction in the planes is intrinsically d-wave and then attempted to assess the influence of coupling to the chains. Closely related to the proximity models are the S/S' multilayer models in which there are two (or more) different superconducting layers in the unit cell. There have been detailed examinations of the roles played by interplane and intraplane pairing[16-18] and a few quantitative calculations of physical properties,[8,16,17] but these models have been less thoroughly explored than the proximity model because of their relative complexity.

In this work we address the issue of whether a proximity model can account for the condensate on the chains in the YBaCuO compounds. We do this by calculating

<u>52</u>   10 601

the penetration depth λ for a simple s or d wave model in the a, b, and c directions. In particular, we are interested in comparing the temperature dependences of λ_a and λ_b with experiment.[5] In our model, the unit cell consists of a CuO_2 plane layer and a CuO chain layer. The CuO_2 planes contain the pairing interaction and are coupled to the CuO chains through coherent single-electron tunneling so that there is an induced gap in the chains. Calculations of the penetration depth in a similar model have been made before,[11,14] although the intrinsically normal layers were planes and not chains, and the emphasis was on the anisotropy between λ_{ab} and λ_c.

In Sec. II we introduce our model Hamiltonian and find the single-particle Green's functions which we will need for the penetration depth. In Sec. III we derive an expression for the penetration depth which is suitable for a two-band, tight binding model. The calculation differs slightly from one we made previously.[14] In Sec. IV we discuss the results of numerical calculations of the penetration depth, and in Sec. V we broaden the scope to a discussion of the nature of the condensate on the chains.

II. HAMILTONIAN

The goal of this section is to introduce our model for YBCO, and to find the single-particle Green's functions necessary for the calculation of the penetration depth in Sec. III. We begin with a Hamiltonian which describes a system with two layers per unit cell. Adjacent layers are separated by a distance $d/2$. The first layer represents a CuO_2 plane and it contains a BCS-like pairing interaction. The second layer represents a CuO chain. It has a one-dimensional dispersion and is intrinsically normal. The chains are superconducting, however, because of their coupling to the planes through single-electron tunneling. The Hamiltonian, expressed in the Nambu formalism, is

$$\mathbf{H} - \mathbf{N}\mu = \sum_{\mathbf{k}} \mathbf{C}^{\dagger}(\mathbf{k}) Q(\mathbf{k}) \mathbf{C}(\mathbf{k}) + \text{const}, \quad (1)$$

where

$$\mathbf{C}(\mathbf{k}) = \begin{bmatrix} c_{1\mathbf{k}\uparrow} \\ c^{\dagger}_{1-\mathbf{k}\downarrow} \\ c_{2\mathbf{k}\uparrow} \\ c^{\dagger}_{2-\mathbf{k}\downarrow} \end{bmatrix} \quad (2)$$

and

$$Q = \begin{bmatrix} \xi_1(\mathbf{k}) & -\Delta_{\mathbf{k}} & t(\mathbf{k}) & 0 \\ -\Delta^*_{\mathbf{k}} & -\xi_1(-\mathbf{k}) & 0 & -t^*(-\mathbf{k}) \\ t^*(\mathbf{k}) & 0 & \xi_2(\mathbf{k}) & 0 \\ 0 & -t(-\mathbf{k}) & 0 & -\xi_2(-\mathbf{k}) \end{bmatrix}. \quad (3)$$

This Hamiltonian has been discussed at length elsewhere[1,13,15] and we only describe it briefly here. The dispersions ξ_1 and ξ_2 are for the plane and chain layers, respectively. We assume tight binding dispersions so that $\xi_1 = -2\sigma_1[\cos(k_x a) + \cos(k_y b)] - \mu_1$ and

$\xi_2 = -2\sigma_2 \cos(k_y b) - \mu_2$, where a and b are the lattice constants in the planes. In optimally doped Y-123 crystals, a and b differ by $\sim 1\%$. For the numerical calculations done in this work, we take $a = b$. We take $\sigma_1 = 100$ meV so that the full bandwidth of the CuO_2 plane is 0.8 eV. For the chain layer we take $\sigma_2 = 80$ meV so that $\lambda^2_a(T = 0)/\lambda^2_b(T = 0) \sim 2.5$, as seen experimentally by Basov et al.[4] The chemical potentials are $\mu_1 = -80$ meV and $\mu_2 = 40$ meV, which yields a Fermi surface that is in qualitative agreement with band structure calculations.[33,34] We have absorbed an arbitrary band offset into the chemical potentials so that $\mu_1 \neq \mu_2$. The chains and planes are coupled by the matrix element $t(k_z) = -t_0 \cos(k_z d/2)$, where $d/2$ is the distance between the chains and planes. The chain-plane coupling affects the penetration depth in two ways. First, $t(k_z)$ determines the c-axis transport properties. In a previous paper[14] we have shown that the ratio $\lambda_c(T = 0)/\lambda_{ab}(T = 0)$ varies inversely with t_0. Second, $t(k_z)$ determines the size of the superconducting gap induced on the chains, which is reflected in the temperature dependence of λ_b. In this work we choose $t_0 = 50$ meV which yields $\lambda^2_c(T = 0)/\lambda^2_a(T = 0) \sim 100$, which is in rough agreement with experimental observations.[19–22]

The final feature of our Hamiltonian is that there is a pairing interaction in the plane which drives the superconducting transition. As we have mentioned above, the chains also become superconducting at T_c through their coupling to the planes. The pairing interaction in the planes has the form $V_{\mathbf{k}\mathbf{k}'} = V\eta_{\mathbf{k}}\eta_{\mathbf{k}'}$ with $\eta_{\mathbf{k}} = 1$ for an s-wave superconductor and $\eta_{\mathbf{k}} = \cos(k_x) - \cos(k_y)$ for a $d_{x^2-y^2}$ superconductor. Since the pairing interaction is separable, the order parameter

$$\Delta_{\mathbf{k}} \equiv \frac{1}{\Omega} \sum_{\mathbf{k}'} V_{\mathbf{k}\mathbf{k}'} \langle c_{1-\mathbf{k}'\downarrow} c_{1\mathbf{k}'\uparrow} \rangle \quad (4)$$

(where Ω is the volume of the crystal) can be written $\Delta_{\mathbf{k}} = \Delta_0 \eta_{\mathbf{k}}$.

Diagonalization of the Hamiltonian leads to four energy bands $E_1 = E_+$, $E_2 = E_-$, $E_3 = -E-$, $E_4 = -E+$ with

$$E^2_{\pm} = \frac{\xi^2_1 + \xi^2_2 + \Delta^2_{\mathbf{k}}}{2} + t^2$$
$$\pm \sqrt{\left[\frac{\xi^2_1 - \xi^2_2 + \Delta^2_{\mathbf{k}}}{2}\right]^2 + t^2[(\xi_1 + \xi_2)^2 + \Delta^2_{\mathbf{k}}]}. \quad (5)$$

In Fig. 1 we show the Fermi surface for a range of k_z values between 0 and π/d. The Fermi surface consists of two surfaces on which E_- vanishes in the normal state. The two surfaces are given by the two solutions to $\xi_1(\mathbf{k})\xi_2(\mathbf{k}) = t(k_z)^2$. When $k_z = \pi/d$, $t(k_z) = 0$ and the two pieces of Fermi surface are those of the isolated chain and plane subsystems. When $t(k_z) \neq 0$, the chain and plane states form hybrid bands whose energies are given by

$$\epsilon_{\pm} = \frac{\xi_1 + \xi_2}{2} \pm \sqrt{\left(\frac{\xi_1 - \xi_2}{2}\right)^2 + t^2},$$
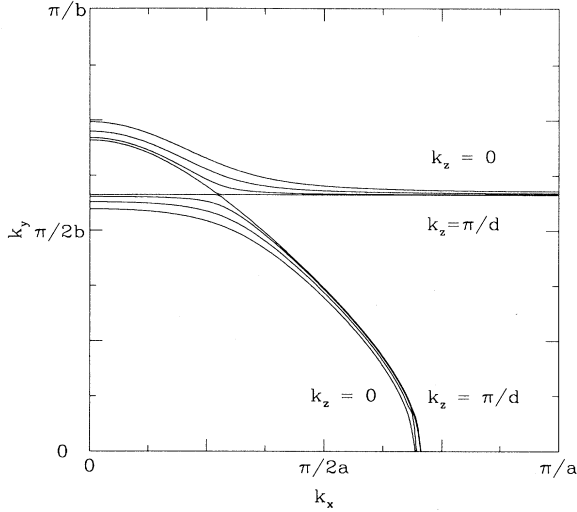
in the normal state. The shift in the band energy due the

FIG. 1. The Fermi surface for the model Hamiltonian is shown for a range of k_z between $k_z = 0$ and $k_z = \pi/d$. When $k_z = \pi/d$, the chain-plane coupling vanishes and the two pieces of Fermi surface are those of the isolated chains and planes. As the chain-plane coupling increases, the Fermi surfaces hybridize and are pushed apart. The effect of the chain-plane coupling is largest where the two Fermi surfaces are closest together. There is an induced gap on the chains whose size is greatest where there is the most chain-plane mixing.

chain-plane coupling is clearly dependent on the relative sizes of t^2 and $(\xi_1 - \xi_2)^2$. The effect of the chain-plane coupling on the Fermi surfaces shown in Fig. 1 is largest in the neighborhood of the Fermi surface crossing at $\xi_1 = \xi_2 = 0$.

The quasiparticle operators in the diagonalized representation are

$$\hat{\mathbf{C}}_i(\mathbf{k}) = \sum_{j=1}^{4} U_{ij}^{\dagger}(\mathbf{k})\mathbf{C}_j(\mathbf{k}), \qquad (6)$$

where $U(\mathbf{k})$ is the 4×4 matrix which diagonalizes Q: $U = [U_1 \, U_2 \, U_3 \, U_4]$ with

$$U_j = \frac{1}{\sqrt{C}} \begin{bmatrix} (E_j - \xi_2)A \\ -(E_j + \xi_2)B \\ tA \\ tB \end{bmatrix}, \qquad (7)$$

$$A = t^2 - (\Delta_{\mathbf{k}} + E_j + \xi_1)(E_j + \xi_2),$$

$$B = t^2 - (\Delta_{\mathbf{k}}^* + E_j - \xi_1)(E_j - \xi_2),$$

$$C = A^2[t^2 + (E_j - \xi_2)^2]$$
$$+ B^2[t^2 + (E_j + \xi_2)^2].$$

Now that we have diagonalized the Hamiltonian, we

can find the single-particle Green's functions which we will require in the following section. Defining the temperature Green's function $G(\mathbf{k}; \tau)_{ij} = -(1/\hbar)\langle \mathbf{T}\mathbf{C}_i(\mathbf{k}; -i\tau)\mathbf{C}_j^{\dagger}(\mathbf{k}; 0)\rangle$, where $\mathbf{T}$ is the fermion time-ordered product, we have

$$G(\mathbf{k}; i\zeta_l)_{ij} = \sum_{m=1}^{4} \frac{U_{im}(\mathbf{k})U_{mj}^{\dagger}(\mathbf{k})}{i\hbar\zeta_l - E_m(\mathbf{k})}, \qquad (8)$$

where

$$G(\mathbf{k}; i\zeta_l)_{ij} = \int_0^{\hbar\beta} d\tau \, e^{i\zeta_l \tau} G(\mathbf{k}; \tau)_{ij},$$

$\zeta_l = (2l+1)\pi/\hbar\beta$ are the fermion Matsubara frequencies and $\beta = 1/k_B T$, where k_B is the Boltzmann constant and T is temperature. In our calculation of the penetration depth we will need

$$G(\mathbf{k}; \tau = 0^-)_{ij} = \frac{1}{\hbar} \sum_{l=1}^{4} U_{il}(\mathbf{k})f[E_l(\mathbf{k})]U_{lj}^{\dagger}(\mathbf{k}), \qquad (9)$$

where $f(x) = 1/[1 + \exp(\beta x)]$.

We finish this section with a brief discussion of our usage of the word "gap." In the model presented above, there is only one order parameter, $\Delta_{\mathbf{k}}$, and it describes the condensate in the CuO_2 planes. For a separable potential, $\Delta_{\mathbf{k}}$ has the symmetry of the pairing interaction. In a multiband material, however, $\Delta_{\mathbf{k}}$ is not simply related to the pair wave function. For example, the anomalous Green's function (which is essentially the pair wave function) in the CuO_2 plane is

$$G(\mathbf{k}; \omega)_{12} = -\frac{\Delta_{\mathbf{k}}(\omega^2 - \xi_2^2)}{(\omega^2 - E_+^2)(\omega^2 - E_-^2)}.$$

Notice that the symmetry of G_{12} is *not* the same as the symmetry of $\Delta_{\mathbf{k}}$. For this reason, the term "gap" is kept distinct from the term "order parameter," which refers to $\Delta_{\mathbf{k}}$. Perhaps the most useful working definition of "gap" is that it is the value of E_- on the Fermi surface. Clearly, by this definition, the gap is $\mathbf{k}$ dependent. In regions of the Brillouin zone where a section of Fermi surface has predominantly chain (or plane) character, the gap can be associated with the chains (or planes). It is wrong to think of the pairs being localized to the chains or planes, however; the pairing amplitude between an electron in the chains and an electron in the planes (measured by G_{14} and G_{23}) is nonzero. In fact the picture of a gap belonging to a plane or a chain breaks down in regions of the Brillouin zone where the Fermi surface is a strong hybridization of the chain and plane bands.

III. PENETRATION DEPTH

The penetration depth is found using an approach which is suitable for the tight binding limit. This approach is slightly different than that of our previous work,[14] although it yields quantitative results which are

nearly identical. As we shall see, however, the current method, which is based on one used by Hirsch and Marsiglio for a one band tight binding model,[23] is more satisfying from a physical point of view.

We begin by writing out the current operator $\mathbf{j_0}$ in the absence of a magnetic field:[24]

$$\mathbf{j_0(q=0)} \equiv \int d^3\mathbf{r}\,\mathbf{j(r)}$$
$$= \frac{ie}{\hbar}[\mathbf{H_0^n, P}], \qquad (10)$$

where

$$\mathbf{P} \sim \sum_{i,\mathbf{R_i}} \mathbf{R_i} c_i^\dagger(\mathbf{R_i}) c_i(\mathbf{R_i}) \qquad (11)$$

is the polarization vector and $\mathbf{H^n}$ is the Hamiltonian in the normal state. The operator $c_i^\dagger(\mathbf{R_i})$ creates an electron in the Wannier state located at the sublattice point $\mathbf{R_i}$. The set of points $\{\mathbf{R_1}\}$ refers to the plane sublattice while $\{\mathbf{R_2}\}$ refers to the chain sublattice. The Wannier representation is connected to the k-space representation by

$$c_i(\mathbf{R_i}) = \frac{1}{\sqrt{N}} \sum_\mathbf{k} e^{i\mathbf{k}\cdot\mathbf{R_i}} c_i(\mathbf{k}), \qquad (12)$$

where N is the number of lattice sites.

In the normal state the Hamiltonian, Eq. (1), can be written in the Wannier representation as

$$\mathbf{H_0^n} = -\sum_{i=1}^2 \sum_{\mathbf{R_i},\mathbf{r_i}} \sigma_i c_i^\dagger(\mathbf{R_i}+\mathbf{r_i})c_i(\mathbf{R_i})$$
$$-\frac{t_0}{2}\sum_{\mathbf{R_1},\mathbf{R_2}}\{c_1^\dagger(\mathbf{R_1})c_2(\mathbf{R_2})[\delta_{\mathbf{R_1}+\hat{z}d/2,\mathbf{R_2}}$$
$$+\delta_{\mathbf{R_1}-\hat{z}d/2,\mathbf{R_2}}] + \text{H.c.}\}. \qquad (13)$$

The vector $\mathbf{r_i}$ is the displacement to the nearest neighbors of $\mathbf{R_i}$ within the plane, $\hat{z}$ is the unit vector in the z direction, and H.c. indicates the Hermitian conjugate. This Hamiltonian describes nearest neighbor hopping both within and between the chains and planes. Substituting Eqs. (11) and (13) into Eq. (10) we get

$$\mathbf{j_0} = \frac{ie}{\hbar}\sum_{i,\mathbf{R_i},\mathbf{r_i}} \sigma_i\,\mathbf{r_i} c_i^\dagger(\mathbf{R_i}+\mathbf{r_i})c_i(\mathbf{R_i})$$
$$-\frac{iet_0d}{4\hbar}\sum_{\mathbf{R_1}}\hat{z}\left[c_1^\dagger(\mathbf{R_1})c_2(\mathbf{R_1}+\hat{z}d/2)\right.$$
$$\left. - c_1^\dagger(\mathbf{R_1})c_2(\mathbf{R_1}-\hat{z}d/2) - \text{H.c.}\right]. \qquad (14)$$

In the presence of a finite magnetic vector potential $\mathbf{A(r)}$, the tight binding Wannier states are modified by a phase so that

$$c_i(\mathbf{R_i}) \to c_i(\mathbf{R_i})\exp\left[-\frac{ie}{\hbar c}\mathbf{R_i}\cdot\mathbf{A(R_i)}\right], \qquad (15)$$

where c is the speed of light. The assumption is made that the vector potential is slowly varying over the length

scale of the crystal lattice, and we will make use of the fact that $\mathbf{A(q)}$ is strongly peaked about $\mathbf{q}=0$ throughout this section. To linear order in $\mathbf{A}$, then, Eq. (13) becomes

$$\mathbf{H^n} = \mathbf{H_0^n} - \frac{1}{c\Omega}\mathbf{j_0}\cdot\mathbf{A(q=0)} \qquad (16)$$

and Eq. (14) becomes

$$\mathbf{j} = \mathbf{j_0} - \frac{e^2}{\hbar^2 c}\sum_{i,\mathbf{R_i},\mathbf{r_i}}\sigma_i\,\mathbf{r_i}[\mathbf{r_i}\cdot\mathbf{A(R_i)}]c_i^\dagger(\mathbf{R_i}+\mathbf{r_i})c_i(\mathbf{R_i})$$
$$-\frac{e^2 t_0 d^2}{8\hbar^2 c}\sum_{\mathbf{R_1}}\hat{z}[\hat{z}\cdot\mathbf{A(R_1)}]\left[c_1^\dagger(\mathbf{R_1})c_2(\mathbf{R_1}+\hat{z}d/2)\right.$$
$$\left. + c_1^\dagger(\mathbf{R_1})c_2(\mathbf{R_1}-\hat{z}d/2) + \text{H.c.}\right]. \qquad (17)$$

In the presence of a magnetic field, the observable current is given by $\langle\mathbf{j}\rangle$, and not $\langle\mathbf{j_0}\rangle$. We can rewrite Eq. (17) in a $\mathbf{k}$ space representation using Eq. (12):

$$\mathbf{j(q=0)} = \frac{e}{\hbar}\sum_\mathbf{k}\left[\mathbf{C^\dagger(k)}\vec{\gamma}_\mathbf{k}\mathbf{C(k)}\right.$$
$$\left. - \frac{e}{\hbar c\Omega}\mathbf{C^\dagger(k)}[\overleftrightarrow{\gamma}_\mathbf{k}'\cdot\mathbf{A(q=0)}]\mathbf{C(k)}\right]. \qquad (18)$$

The vector $\vec{\gamma}_\mathbf{k}$ is a 4×4 matrix with three spatial components. It is essentially the Fermi velocity

$$\vec{\gamma}_{\mathbf{k}ij} = (-1)^{i-1}\frac{\partial Q_{ij}}{\partial\mathbf{k}},$$

where Q_{ij} is the Hamiltonian matrix of Eq. (3) and the factor $(-1)^{i-1}$ comes from the fact that $\mathbf{C}_i$ annihilates electron states for $i=1,3$ and hole states for $i=2,4$. The dyadic $\overleftrightarrow{\gamma}_\mathbf{k}'$ is also a 4×4 matrix and it is essentially the effective mass tensor

$$\overleftrightarrow{\gamma}_{\mathbf{k}ij}' = \frac{\partial^2 Q_{ij}}{\partial\mathbf{k}\partial\mathbf{k}}.$$

The first term in Eq. (18) is $\mathbf{j_0(q=0)}$ while the second term contains the remaining two terms in Eq. (17).

The current $\langle\mathbf{j}\rangle$ which is generated by the applied magnetic field is given, to linear order in $\mathbf{A}$, by the Kubo formula[25]

$$\langle\mathbf{j}(t)\rangle = \langle\mathbf{j}(t)\rangle_0 + \frac{i}{\hbar}\int_{-\infty}^t dt'\left\langle\left[-\frac{1}{c}\mathbf{j_0}(t')\cdot\mathbf{A}(t'),\mathbf{j_0}(t)\right]\right\rangle_0.$$

In the London limit, for the case of a static applied field, this gives

$$\langle\mathbf{j(r)}\rangle = \langle\mathbf{j(r)}\rangle_0 - \frac{1}{c\Omega}\sum_\nu G_{\mu\nu}^j(0,0;0)A_\nu(\mathbf{r}), \qquad (19)$$

where

$$G_{\mu\nu}^j(\mathbf{q},\mathbf{q}',i\omega_l) = -\frac{1}{\hbar\Omega}\int_0^{\hbar\beta} d\tau\, e^{i\omega_l\tau}$$
$$\times\langle\mathbf{T}j_{0\mu}(\mathbf{q},-i\tau)j_{0\nu}(\mathbf{q}',0)\rangle_0.$$

G^j is the current-current correlation function, $\mathbf{T}$ is the

boson time-ordered product, $\omega_l = 2l\pi/\hbar\beta$ are the boson Matsubara frequencies, and μ and ν refer to the spatial components of $\mathbf{j_0}$. The expectation values $\langle\rangle_0$ are taken with respect to the zero-field wave function. It is straightforward to evaluate G^j in terms of the single-particle Green's functions:

$$G^j_{\mu\nu}(0,0;i\omega_l) = \lim_{\mathbf{q}\to 0} \frac{e^2}{\beta\hbar^2\Omega} \sum_{n,\mathbf{k}} \mathrm{Tr}\,[G(\mathbf{k};i\zeta_n - i\omega_l)\vec{\gamma}_{\mathbf{k}\mu}$$

$$\times\, G(\mathbf{k}+\mathbf{q};i\zeta_n)\vec{\gamma}_{\mathbf{k}\nu}]\,. \tag{20}$$

The first term in Eq. (19) is the diamagnetic contribution to the screening current. Using Eqs. (9) and (18) we may evaluate this explicitly:

$$\langle\mathbf{j(r)}\rangle_{\mathrm{dia}} = \frac{1}{\Omega} \sum_{\mathbf{q}} \langle\mathbf{j(q)}\rangle_{\mathrm{dia}}\, e^{i\mathbf{q}\cdot\mathbf{r}}$$

$$= \frac{e^2}{\Omega\hbar c} \sum_{\mathbf{k}} \mathrm{Tr}\,[G(\mathbf{k};\tau = 0^-)\overset{\leftrightarrow}{\gamma}'_{\mathbf{k}}]\cdot\mathbf{A(r)}$$

$$= \frac{e^2}{\Omega\hbar^2 c} \sum_{\mathbf{k}} \sum_{i=1}^{4} f[E_i(\mathbf{k})]\hat{\gamma}'_{\mathbf{k}ii}\cdot\mathbf{A(r)}, \tag{21a}$$

where Tr is a trace over the components of the 4×4 matrix contained in the square brackets, and $\hat{\gamma}'_{\mathbf{k}} = U^\dagger(\mathbf{k})\overset{\leftrightarrow}{\gamma}'_{\mathbf{k}}U(\mathbf{k})$. In order to derive Eq. (21a), we have used the fact that $\langle\mathbf{j_0}\rangle_0 = 0$ and that $\mathbf{A(q)}$ is peaked about $\mathbf{q} = 0$. The second term in Eq. (19) is the paramagnetic contribution to the screening current. Evaluating Eq. (20) explicitly we have

$$\langle\mathbf{j}\rangle_{\mathrm{para}} = -\frac{e^2}{\Omega\hbar^2 c} \sum_{i,j=1}^{4} \sum_{\mathbf{k}} \hat{\gamma}_{\mathbf{k}ij}[\hat{\gamma}_{\mathbf{k}ji}\cdot\mathbf{A(r)}]$$

$$\times \left[\delta_{i,j}\frac{\partial f(E_i)}{\partial E_i}\right.$$

$$\left.+[1-\delta_{i,j}]\frac{f(E_i)-f(E_j)}{E_i-E_j}\right], \tag{21b}$$

where $\hat{\gamma}_{\mathbf{k}} = U^\dagger(\mathbf{k})\vec{\gamma}_{\mathbf{k}}U(\mathbf{k})$. This expression for the paramagnetic current is the same as in Ref. 14 where it was discussed at length. We will only repeat the points which are directly relevant to the current work, and the interested reader is referred to our earlier work. The total current produced by the magnetic field is

$$\langle\mathbf{j}\rangle = \langle\mathbf{j}\rangle_{\mathrm{dia}} + \langle\mathbf{j}\rangle_{\mathrm{para}}$$

$$= -\mathbf{K}\cdot\mathbf{A}. \tag{22}$$

It is straightforward to show that $\mathbf{K}_{\mu\nu} = 0$ if $\mu \neq \nu$ (recall that μ and ν refer to spatial directions) so that the penetration depth is given by

$$\frac{1}{\lambda_\mu^2} = \mathbf{K}_{\mu\mu}. \tag{23}$$

This is the main result for this section. In order to plot λ_μ^{-2} as a function of temperature in Sec. IV, we must evaluate the integrals in Eqs. (21a) and (21b) numerically.

We will finish this section with a few comments about Eqs. (21a) and (21b). In the usual treatment of the penetration depth the diamagnetic contribution to the screening current is $\mathbf{j}_{\mathrm{dia}} = -ne^2\mathbf{A}/mc$, which is independent of temperature. The temperature dependence of the penetration depth, then, comes from the paramagnectic contribution to the screening currents which, for a one-band free electron metal with an isotropic gap, is

$$\mathbf{j}_{\mathrm{para}} = -\frac{ne^2}{2\mu\hbar c} \int_{-\mu}^{\infty} d\epsilon\,[v^f]^2\,\frac{\partial f(E)}{\partial E}, \tag{24}$$

where $E = [\epsilon^2 + \Delta^2]^{1/2}$, v^f is the Fermi velocity, and μ is the chemical potential. The paramagnetic term counts the number of thermal excitations (broken Cooper pairs) which degrade the screening current. At $T = 0$ the paramagnetic term vanishes, so that $\mathbf{j} = -ne^2\mathbf{A}/mc$. When $\Delta = 0$ the paramagnetic term cancels the diamagnetic term exactly so that $\mathbf{j} = 0$. For systems which are more complicated than the free electon gas, it is common to make the approximation $\mathbf{j}_{\mathrm{dia}} = -\mathbf{j}_{\mathrm{para}}|_{\Delta=0}$. The approximation is exact at $T = T_c$ and, provided the temperature dependence of the diamagnetic term is weak, the approximation is a good one. This is the approximation we made in our previous discussion of the two-layer model.[14] In the current work, however, we have treated $\mathbf{j}_{\mathrm{dia}}$ in a fashion which is more consistent with the tight binding model, so that while Eq. (21b) is the same as we found previously, Eq. (21a) is different. There is little quantitative difference between the two approaches, however, since both expressions for the diamagnetic current are weakly temperature dependent and both cancel the paramagnetic current above T_c.

The most significant difference between Eq. (21a) and the usual expression for the penetration depth is the interband term, which is proportional to $[f(E_i) - f(E_j)]/[E_i - E_j]$. While the intraband term [which is proportional to $\partial f(E_i)/\partial E_i$] counts the number of thermally broken pairs, the interband term describes the degradation of the screening currents by interband transitions. The interband term does not vanish at $T = 0$ so that, unlike the single band case, there is a finite paramagnetic contribution to the screening current.

IV. RESULTS

The question we are attempting to address in this work is whether a proximity effect model can account for the experimentally observed anisotropy in the temperature dependence of the penetration depth in Y-123. In this section we will present the results of numerical calculations of the penetration depth for the model Hamiltonian introduced in Sec. II. We will compare these results to experiments and to related calculations made with a two-plane proximity model (in which the intrinsically normal layer is a two-dimensional plane). One of the main goals of this section is to emphasize the difference between two-plane proximity models and chain-plane models of the

type studied here.

To begin with, we will discuss calculations of the penetration depth in the two-plane proximity models.[11,14] One of the important features of the proximity model is that it introduces low energy excitations into the superconducting spectrum. The reason for this is that the induced gap in the intrinsically normal plane is proportional to the strength of the chain-plane coupling $t(k_z)$ (which vanishes at $k_z = \pi/d$) so that the gap will have a nodal structure even if the pairing interaction has isotropic s-wave symmetry. The need for a gap structure with nodes has been suggested, for example, by measurements[26] of λ_{ab} (the in-plane penetration depth) in twinned single crystals of Y-123. The linear dependence of $\lambda_{ab}(T)$ on T at low temperatures is easily explained by any gap structure with nodes.[29] While these measurements are commonly taken as support for d-wave models,[28] it has also been shown[11,14] that two-plane proximity models also result in linear low T behavior. Since a central theme in much of the work on proximity models[1,7–10,12,16] is that the pairing interaction in the intrinsically superconducting plane is s-wave, the low energy excitations in the induced gap are an essential feature of the proximity models.

In Fig. 2(a) we plot the penetration depth for our plane-chain proximity model for the case of an s-wave gap. We find that, unlike the case of the two-plane model, the temperature dependences of λ_a and λ_b are dramatically different. The most important difference is that the temperature dependence of λ_a is nearly identical to that of a single-layer s-wave material with no chains, while λ_b has a linear low T behavior similar to that found in the two-plane proximity models.[14] The factor of 2 difference between $\lambda_a(0)^{-2}$ and $\lambda_b(0)^{-2}$ comes from the screening currents carried in the b direction by the chains, and the linear T dependence in λ_b^{-2} at low temperatures comes from the node in the induced gap at $k_z = \pi/d$. The fact

that the low T behavior of λ_a^{-2} is exponential and not linear indicates that pairs associated with a axis screening currents have a finite gap for all values of k_z. We can understand this in more concrete terms as follows: In Sec. III we showed that the screening current has two parts—a diamagnetic part which is roughly independent of T and a paramagnetic part which accounts for processes (such as thermal pair breaking) which degrade the screening currents. The temperature dependence of the penetration depth comes from the paramagnetic screening current, given in Eq. (21a). Despite its complicated appearance, Eq. (21b) has a simple physical interpretation. The factors $\hat{\gamma}_{\mathbf{k}}$ are electron Fermi velocity *vectors*, while the two terms involving Fermi functions count the number of thermally excited quasiparticles which participate in intraband $(i = j)$ or interband $(i \neq j)$ paramagnetic processes. When we calculate the screening current in the a direction, then, the integrand in Eq. (21b) is weighted by the square of the Fermi velocity in the a direction. In Fig. 1, we can see that this is small both on segments of the Fermi surface associated with the chains and on segments of the plane Fermi surface which are distorted by the chains. The most obvious consequence of this is that the chains do not participate significantly in carrying currents in the a direction. A more subtle result is that, even though there is a node in the induced gap in the chains, it is not seen by electrons traveling in the a direction so that Cooper pairs which are part of the a axis screening current have a finite gap. The onset of thermal pair breaking, then, occurs at a much lower temperature in the b axis supercurrent than in the a axis supercurrent.

In Fig. 2(b) we plot the penetration depth for a d-wave order parameter and find results which are similar to the s-wave case: $\lambda_a(T)$ is essentially the same as found in single-layer d-wave models and $\lambda_b(T)$ resembles $\lambda_{ab}(T)$ found in the two-plane proximity models. As for the
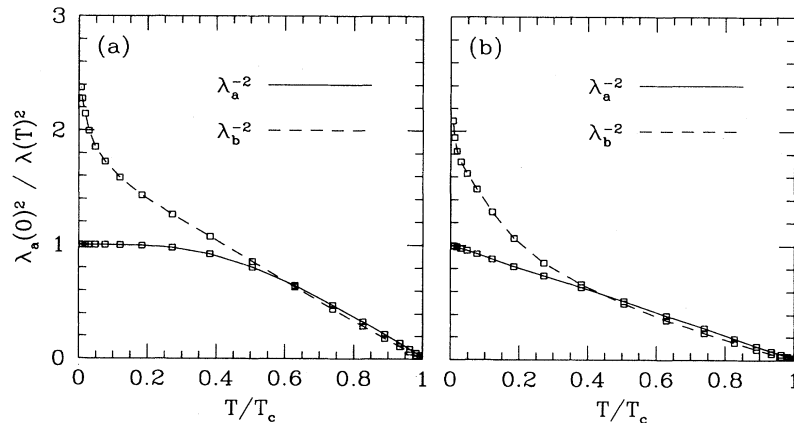

FIG. 2. (a) In-plane penetration depth for an s-wave order parameter. The penetration depth in the a direction (perpendicular to the chains) is nearly that of a pure s-wave superconductor in the absence of chains. The penetration depth in the b direction has a very different temperature dependence from that in the a direction because the size of the induced gap in the chains is much different from the size of the gap in the planes. The relative bandwidths of the chains and planes were determined by setting $\lambda_a^2(0)/\lambda_b^2(0) \sim 2.5$, in accordance with experiment. (b) In-plane penetration depth for a d-wave order parameter. Again, $\lambda_a(T)$ is essentially the same as for a single-layer d-wave superconductor, while the shape of $\lambda_b(T)$ reflects the structure of the induced gap in the chains as well as the planes.

case of an s-wave gap, the reason is that there are a larger number of low energy excitations in the chains than in the planes. The d-wave gap in the planes has nodes along $k_x = \pm k_y$, while the induced gap has nodes along $k_x = \pm k_y$ and $k_z = \pi/d$.

The large temperature dependence of the ab anisotropy seen in Figs. 2(a) and 2(b) is difficult to reconcile with measurements of $\lambda_a(T)$ and $\lambda_b(T)$ in untwinned crystals. In these experiments[5] λ_a and λ_b have a nearly identical temperature dependence, although their absolute magnitude differs by a factor of 1.5 at $T = 0$. In our model, the temperature dependence of the anisotropy is a result of the fact that Cooper pairs in the chains are more easily broken than Cooper pairs in the planes. Clearly, then, in a realistic model, the density of low energy excitations in the chains must be similar to that in the planes. This is not a trivial requirement. It implies that both the nodal structure and the magnitude of the gaps in the chains and planes be similar. It is possible to eliminate the nodes in the induced gap at $k_z = \pi/d$ by, for example, making the ansatz that $t(k_z) = t_0$ (this would describe a single bilayer). However, this is not sufficient to eliminate the temperature dependence of the anisotropy. For regions of the chain Fermi surface where $|\xi_1| \gg |t(k_z)|$, the induced gap is of the order[14] $\Delta_{\mathbf{k}} t(k_z)^2/\xi_1^2$. In Fig. 1, the smallest induced gap occurs at the intersection of the chain Fermi surface with the Brillouin zone boundary (at $k_x = \pi/a$) at which $t_0^2/\xi_1(\mathbf{k})^2 \sim 0.023$. The onset of thermal pair breaking in the chains, therefore, will occur at a much lower temperature than in the planes.

The penetration depth in the c direction as a function of temperature is shown in Fig. 3. The shapes of the curves are similar to what we found in previous work[14] in which we examined a model with two planes per unit cell. Experimental observations of λ_c in Y-123 (Refs. 20, 22, and 29 and Y-124[19]) are contradictory. All of the experi-

ments find that at low temperatures $\lambda_c^{-2}(T)$ can be fitted by a linear T dependence, $\lambda_c(0)^2/\lambda_c(T)^2 \sim 1 - \alpha T/T_c$, but the slope of the fit varies dramatically. Two of the infrared experiments[19,22] find that $\alpha \ll 1$, while the third[29] finds that $\alpha \sim 1$ and the microwave experiment[20] finds that $\alpha \gg 1$. Until some sort of consensus is achieved, it will be difficult to say anything about our model.

V. CONCLUSIONS

It is clear that our proximity effect model cannot describe the temperature dependence of the ab anisotropy of the penetration depth which has been observed experimentally by Zhang $et~al.$[5] Essentially, the problem with our proximity model is that, unlike the case of the two-plane model, there are always regions of the chain Fermi surface on which the gap is small, so that the temperature scale over which the penetration depth parallel to the chains varies is much lower than the scale perpendicular to the chains. The question that needs to be answered, then, is to what extent is our model representative of proximity models in general.

The common feature of proximity models is that the chains are intrinsically normal but driven superconducting by their coupling to the planes. Where proximity models differ is in the nature of the chain-plane coupling. In our model we have made the assumption that the chain-plane coupling is coherent, so that chain states are coupled to plane states with the same value of $\mathbf{k}$. The amount of mixing between the two states depends on the difference in energy between them so that, for example, in Fig. 1 the chain and plane Fermi surfaces are most strongly mixed in the neighborhood of their crossing. In a similar fashion, the induced gap on the chain is small (of the order of a few percent of the intrinsic gap in the plane) wherever the chain and plane Fermi surfaces are far apart. This is the reason for the large difference in the temperature dependence of λ_a and λ_b.

One solution to this is to couple the chains and planes incoherently, so that every state $\mathbf{k}$ on the planes is coupled equally to every state $\mathbf{k}'$ on the chains. There is some evidence that there is incoherence along the c axis: Kleiner and Müller[30] have found an intrinsic Josephson effect in $Bi_2Sr_2CaCu_2O_8$ and, more recently, in underdoped Y-123. The dc resistivity of Y-123 in the normal state[3] shows semiconducting behavior in underdoped samples, and the optical conductivity along the c axis (see, e.g., Ref. 22, and references contained therein) has a nonmetallic response. For an incoherent model of the type described above, the induced gap on the chains is proportional to the average over the Fermi surface of the gap on the planes. The difficulty with this model is that, for a d-wave order parameter, the induced gap in the chains will vanish. It is, in fact, a general feature of d-wave order parameters that they do not contribute to incoherent processes (see, for example, Refs. 31 and 15). If on the other hand, we assume that the order parameter in the planes has an isotropic s-wave symmetry, then the induced gap on the chains will not vanish. The problem
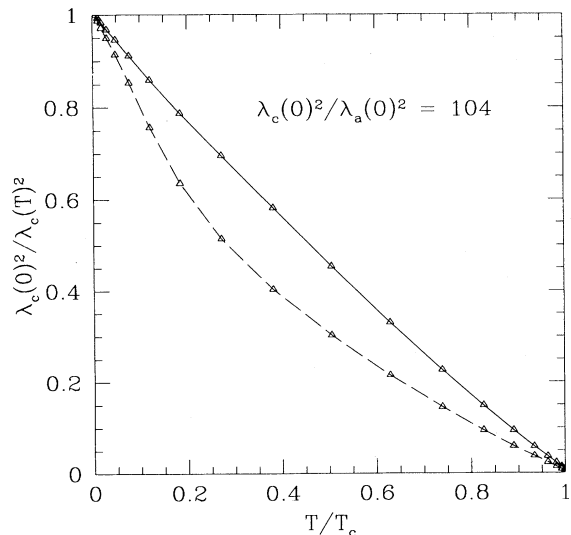

FIG. 3. Penetration depth in the c direction for both an s-wave (solid line) and a d-wave (dashed line) order parameter. The strength of the chain-plane coupling is chosen to be $t_0 = 50$ meV so that $\lambda_c^2(0)/\lambda_a^2(0) \sim 100$, as observed experimentally.

now, however, is that incoherent coupling does not introduce a nodal structure into the gap the way coherent coupling does so that it is difficult to reconcile such a model with a linear low temperature penetration depth. For a model with incoherent chain-plane coupling to successfully describe the low temperature penetration depth, it would have to have an order parameter with nodes on the Fermi surface but whose Fermi surface average was nonzero, and the induced gap in the chains would have to be of the order of T_c so that the temperature dependence of λ_a and λ_b would be similar.

Leaving, for a moment, the discussion of the nature of the chain-plane coupling, we will now turn to a more conceptual problem–that of the size of the chain-plane coupling. The coupling strength t_0 is chosen to account both for the fact that $\lambda_c(T = 0)/\lambda_a(T = 0) \sim 10$ (Refs. 19–22) and for the size of the induced gap in the chains. As is well known, the chain-plane coupling can degrade T_c substantially. We find that for $t_0 = 50$ meV, T_c is only 65% of its value at $t_0 = 0$. It is also difficult to reconcile the picture of weakly coupled two-dimensional planes with such large values of the chain-plane coupling. In our model the ratio of the electron hopping strengths along the c and in-plane directions is $t_0/2\sigma_1 = 0.25$, so that it is difficult to imagine that the c axis coupling is a weak perturbation in an otherwise two-dimensional system. The challenge, therefore, for theories which begin with models of a single CuO_2 plane is to explain the large anisotropy between the a and b supercurrents in YBCO without invoking a large chain-plane coupling.

Kresin and Wolf[12] have suggested that proximity effect models require an inelastic channel for the chain-plane coupling. In their two-plane model, electrons can hop between the planes through coherent tunneling or through scattering from a phonon. Their model is more three-dimensional than the ones discussed above since the inelastic interplane coupling acts as a pairing process which leads to an increase in T_c. It is possible that in a chain-plane model, some kind of inelastic transport mechanism along the c axis might lead to a sufficiently large gap in

the chains that λ_a and λ_b would have similar T dependences. The idea of a mixture of pairing interactions has recently been proposed by Song and Annett,[32] although they have limited their discussion to mixing phonons and Coulomb interactions within a single plane.

There is also the issue of whether a simple two-band model can be representative of Y-123. More careful band structure calculations[33,34] find that the Fermi surface has four pieces instead of two. The two additional pieces of Fermi surface come from the internal structure of the CuO_2 bilayer (which we have treated as a single-layer) and from the internal structure of the CuO chains. The inclusion of these two pieces of Fermi surface is not likely to affect the important results contained within this paper however: the additional piece of Fermi surface due to the CuO_2 bilayer has a nearly tetragonal symmetry (and will therefore not contribute to the anisotropy in the penetration depth) and the piece due to the CuO chains is small and will only make a small change to the screening currents.

Our final conclusion, then, is as follows: A proximity model for Y-123 in which the superconducting pairing interaction is localized to the planes and the chain-plane coupling is coherent will not account for the temperature dependence of the anisotropy of the penetration depth seen in experiments. It is possible that other models for the chain-plane coupling will be able to adequately describe the ab anisotropy. The single largest problem faced by proximity models is that penetration depth experiments[5] seem to indicate that the gap in the chains is of the same order as the gap in the planes.

ACKNOWLEDGMENTS

[1] A. A. Abrikosov, Physica C **182**, 191 (1991); A. A. Abrikosov and R. A. Klemm, *ibid.* **191**, 224 (1992).

[2] T. A. Friedmann *et al.*, Phys. Rev. B **42**, 6217 (1990).

[3] R. Gagnon, C. Lupien, and L. Taillefer, Phys. Rev. B **50**, 3458 (1994).

[4] D. N. Basov *et al.*, Phys. Rev. Lett. **74**, 598 (1995).

[5] K. Zhang *et al.*, Phys. Rev. Lett. **73**, 2484 (1994).

[6] J. L. Tallon *et al.*, Phys. Rev. Lett. **74**, 1008 (1995).

[7] M. Tachiki, S. Takahashi, F. Steglich, and H. Adrian, Z. Phys. B **80**, 161 (1990); M. Tachiki, T. Koyama, and S. Takahashi, Prog. Theor. Phys. Suppl. **108**, 297 (1992); S. Takahashi and M. Tachiki, Physica C **170**, 505 (1990).

[8] A. I. Buzdin, V. P. Damjanović, and A. Yu. Simonov, Phys. Rev. B **45**, 7499 (1992); Physica C **194**, 109 (1992).

[9] L. N. Bulaevskii and M. V. Zyskin, Phys. Rev. B **42**, 10 230 (1990).

[10] A. Yu. Simonov, Physica C **211**, 455 (1993).

[11] R. A. Klemm and S. H. Liu, Phys. Rev. Lett. **74**, 2343 (1995).

[12] V. Z. Kresin, H. Morawitz, and S. A. Wolf, *Mechanisms of Conventional and High T_c Superconductivity* (Oxford University Press, Oxford, 1993); V. Z. Kresin and S. A. Wolf, Phys. Rev. B **51**, 1229 (1995).

[13] W. A. Atkinson and J. P. Carbotte, Phys. Rev. B **51**, 1161 (1995)

[14] W. A. Atkinson and J. P. Carbotte, Phys. Rev. B **51**, 16 371 (1995).

[15] W. A. Atkinson and J. P. Carbotte, Phys. Rev. B **52**, 6894 (1995).

[16] S. H. Liu and R. A. Klemm, Phys. Rev. B **45**, 415 (1992); R. A. Klemm and S. H. Liu, Physica C **191**, 383 (1992); **216**, 293 (1993).

[17] T. Schneider, H. De Raedt, and M. Frick, Z. Phys. B **76**, 3 (1989).

[18] S. Kettemann and K. B. Efetov, Phys. Rev. B **46**, 8515 (1992).

[19] D. N. Basov, T. Timusk, B. Dabrowski, and J. D. Jorgensen, Phys. Rev. B **49**, 3511 (1994).

[20] J. Mao, D. H. Wu, J. L. Peng, R. L. Greene, and S. M. Anlage, Phys. Rev. B **51**, 3316 (1995).

[21] J. Schützmann, S. Tajima, S. Miyamoto, and S. Tanaka, Phys. Rev. Lett. **73**, 174 (1994).

[22] C. C. Homes, T. Timusk, D. A. Bonn, R. Liang, and W. N. Hardy (unpublished).

[23] J. E. Hirsch and F. Marsiglio, Phys. Rev. B **45**, 4807 (1992).

[24] G. D. Mahan, *Many-Particle Physics* (Plenum Press, New York, 1986), p. 30.

[25] G. Rickayzen, *Green's Functions and Condensed Matter* (Academic Press, San Diego, 1980), p. 8.

[26] W. N. Hardy *et al.*, Phys. Rev. Lett. **70**, 3999 (1993).

[27] J. Annett, N. Goldenfeld, and S. R. Renn, Phys. Rev. B **43**, 2778 (1991).

[28] M. Prohammer and J. P. Carbotte, Phys. Rev. B **43**, 5370 (1991).

[29] J. Münzel *et al.*, Physica C **235-240**, 1087 (1994).

[30] R. Kleiner and P. Müller, Phys. Rev. B **49**, 1327 (1994); P. Müller, Bull. Am. Phys. Soc. **40**, 376 (1995).

[31] R. J. Radtke, C. N. Lau, and K. Levin (unpublished).

[32] J. Song and J. F. Annett, Phys. Rev. B **51**, 3840 (1995).

[33] W. E. Pickett, H. Krakauer, R. E. Cohen, and D. J. Singh, Science **255**, 46 (1992); W. E. Pickett, R. E. Cohen, and H. Krakauer, Phys. Rev. B **42**, 8764 (1990).

[34] J. Yu, S. Massida, A. J. Freeman, and D. D. Koelling, Phys. Lett. A **122**, 203 (1987).